Phase evolution and magnetic properties of a high-energy ball-milled hematite–alumina system

L. F. Cótica, S. C. Zanatta, M. A. Rocha, I. A. Santos, A. Paesano Jr., J. B. M. da Cunha, and B. Hallouche

Citation: Journal of Applied Physics **95**, 1307 (2004); doi: 10.1063/1.1636262
View online: http://dx.doi.org/10.1063/1.1636262
View Table of Contents: http://scitation.aip.org/content/aip/journal/jap/95/3?ver=pdfcov
Published by the AIP Publishing

Phase evolution and magnetic properties of a high-energy ball-milled hematite–alumina system

L. F. Cótica, S. C. Zanatta, M. A. Rocha, I. A. Santos, and A. Paesano, Jr.[a)]
Departamento de Física, Universidade Estadual de Maringá, Av. Colombo 5790, Maringá PR, Brazil, 87020-900

J. B. M. da Cunha
Instituto de Física, Universidade Federal do Rio Grande do Sul, Porto Alegre RS, Brazil

B. Hallouche
Departamento de Química e Física, Universidade de Santa Cruz do Sul RS, Brazil

(Received 11 March 2003; accepted 30 October 2003)

The system $(\alpha\text{-}Fe_2O_3)_x(\alpha\text{-}Al_2O_3)_{1-x}$ was subjected to 24 h of high-energy ball-milling varying its nominal concentration, x. The milled samples were structurally and magnetically characterized at room temperature by x-ray diffraction, Mössbauer spectroscopy, and magnetic measurements. Mössbauer studies were also performed in the temperature range 250–6 K. As a result of the earlier analyses, it was observed that the milling products were extremely dependent on the hematite starting concentration. In samples with low α-Fe_2O_3 initial concentration (i.e., $x \leqslant 0.12$), the paramagnetic solid solution α-$(Fe_{\Delta Y}Al_{1-\Delta Y})_2O_3$, the α-Fe and the $FeAl_2O_4$ phases were identified, along with alumina, which was always residual. The presence of spinel and metallic iron was attributed to the stainless-steel vial and balls abrasion. For $x > 0.12$, the iron component was no longer present but another magnetic component, corresponding to an aluminum-substituted hematite phase, α-$(Fe_{1-\Delta W}Al_{\Delta W})_2O_3$, could be seen to increase with increasing x. This solid solution was shown to be transitional, at room temperature, between two ordering states, weak ferromagnetic and superparamagnetic, the latter resulting from the milling induced particle size reduction. Low temperature Mössbauer spectra revealed the magnetic ordering of both solid solutions, α-$(Fe_{\Delta Y}Al_{1-\Delta Y})_2O_3$ and α-$(Fe_{1-\Delta W}Al_{\Delta W})_2O_3$, and indicated the suppression of the Morin transition for the iron-rich solid solution. The magnetization versus magnetic field curves obtained for samples with $x \geqslant 0.12$ revealed, besides a general superparamagnetic character, some hysteretic behavior due to the magnetic phases eventually existing. © *2004 American Institute of Physics.* [DOI: 10.1063/1.1636262]

I. INTRODUCTION

The high-energy ball-milling technique has emerged as an inexpensive route to produce nonequilibrium phases in several varied forms such as nanostructured and amorphous materials, nanocomposites and extended solid solutions.[1] This preparation technique has attracted much attention because it permits study of metal–metal, oxide–metal, and oxide–oxide solid solutions, which can be metastably extended.[2] The final ball-milled products are usually of nanoscopic scale and are characterized by high surface area, high defect density, and enhanced diffusion rates. In fact, the ball-milled activated materials become, in most cases, more reactive and capable of faster reactions than the thermochemically activated ones.[3] This occurs due to the introduction of free energy in the crystal lattice during the milling process, when the raw materials are submitted to fracturing, deformation and welding.[2–4] For this reason, the milling medium (i.e., the vial and the balls) acquires an important character in the mechanochemical process constituting, with other mechanical settings, a crucial set of parameters to produce materials with desired properties.[1]

To date, a long list of systems has been processed by high-energy ball-milling.[1] Oxides in particular, have been largely investigated mainly focusing on their magnetic, ferroelectric, and refractory properties.[1] A number of techniques have been applied in the above investigations, such as x-ray diffraction (XRD), magnetization, ^{57}Fe Mössbauer spectroscopy (MS), scanning electron microscopy, and transmission electron microscopy, which give structural and macroscopic magnetic information.[1] Ordinarily, microscopic probing of samples provides a more profitable analytical methodology because properties of ball-milled materials are strongly affected by the local mean composition, defects, strain, and average interatomic distances. The mechanically induced changes certainly influence the chemical bonds and, consequently, the magnetic and electric fields around the atoms. ^{57}Fe Mössbauer spectroscopy, being highly responsive to the hyperfine fields at the probe nuclei, becomes a powerful tool in the study of ball-milled materials. Indeed, due to its high energy resolution and detection character of low relaxation

[a)]Electronic mail: paesano@wnet.com.br

time, it provides relevant information concerning the identification of the low level iron containing phases, being much more sensitive to their identification than most of the structural characterization techniques. In addition, it permits the possibility of observing magnetic phase transitions through the magnetic hyperfine field (B_{hf}) evolution. Furthermore, MS also allows studying structural and electronic properties through the other hyperfine parameters. Specifically, the isomer shift (δ) provides a direct measurement of the nuclear electronic density, giving important information about the valence state of the iron atom, while the quadruple splitting (QS) permits study of bounded properties, electronic and molecular structural problems, and possible lattice distorted states, as observed in the ball-milled products. This explains why milled iron compounds can be suitably characterized by Mössbauer spectroscopy.

Hematite (α-Fe_2O_3), for instance, which has important magnetic properties, has been studied extensively, using various techniques including the earlier spectroscopy technique, when individually milled in high-energy ball mills.[5–10] Exploring and understanding the magnetic and electric modifications associated with the structural evolution in the ball-milled hematite, has been the driving force of many efforts conducted in recent years.[7–10]

The crystal structure of hematite is isomorphous to alumina (α-Al_2O_3=corundum), with a close-packed oxygen lattice and Fe^{3+} cations in octahedral sites. It is a complex magnetic material, being antiferromagnetic (AF) at low temperatures and undergoing a transition to a weak ferromagnetic state (WF) above the so-called Morin temperature ($T_M \cong 260$ K), because of a spin canting.[11] The hematite magnetic behavior is very sensitive to strain, external fields and, especially, to impurities or foreign atoms.[12]

In this sense, some researchers have also investigated the products of hematite milled with different metals and oxides.[13] The great technological and academic interest in these composites is due to numerous potential applications, mainly in electronics, metallurgy, and catalysis of ammonia synthesis.[9,14] Surprisingly, so far, in spite of the immense technological and academic importance of the hematite–alumina system, no research concerning the systematic study of this system, prepared through the high-energy ball-milling technique, has been reported in the literature. Actually, the influence of the substitution of aluminum ions on hematite or other iron oxides has already been largely studied.[15,16] However, the characterized samples were prepared by conventional ceramic preparation methods. Therefore, this opens the possibility of applying innovative processing routines, searching for materials with original and optimized properties.

In this context, the aim of this contribution is to analyze the reactions and possible phase transformations induced by high-energy ball milling of the hematite–alumina system. The obtained products were characterized by XRD, magnetization measurements and, principally, MS, focusing on identifying the formed phases and their magnetic behavior.

II. EXPERIMENT

$(Fe_2O_3)_x(Al_2O_3)_{1-x}$ composites were prepared in a Fritsch Pulverisette 6 planetary ball mill, using a 80 cm^3 stainless-steel vial charged with 10 mm diameter stainless-steel balls. Analytical grade α-Fe_2O_3 (99.9%) and α-Al_2O_3 (99.8%) powders were used as precursors. The powders were manually premixed in nominal compositions ranging from $x=0.02$ up to $x=0.50$ and milled in argon atmosphere without any additives (dry milling) and under closed milling conditions, i.e., the vial was not opened during the milling process. The milling settings, i.e., the ball-to-powder-mass ratio (30:1), angular velocity of the supporting disc and vial ($31.42\ rad\ s^{-1}$) and milling time (24 h) were kept constant throughout the experiments. The XRD patterns of the milled products were obtained at RT, using a Siemmens D500 x-ray diffractometer in Bragg–Brentano geometry, with Cu K_α radiation, in the $20° \leqslant 2\theta \leqslant 60°$ range. The MS characterizations were performed in the transmission geometry, using a conventional Mössbauer spectrometer in a constant acceleration mode. The γ-rays were provided by a nominal 10 mCi ^{57}Co(Rh) source. A liquid nitrogen/helium cryostat was used for low-temperature measurements. The Mössbauer spectra were analyzed with a nonlinear least-square routine, with Lorentzian line shapes. All isomer shift (δ) data are given relative to α-Fe throughout this article. Magnetization measurements were performed using a homemade vibrating sample magnetometer, at room temperature.

III. RESULTS AND DISCUSSIONS

XRD patterns for some representative samples are shown in Fig. 1. As can be seen for $x=0.02$ [Fig. 1(a)], the diffraction peaks were assigned as being for alumina and α-Fe. The peak for the $\langle 110 \rangle$ iron plane is observed up to $x=0.12$ [Fig. 1(b)], where some hematite diffraction peaks start to appear. We believe that the iron originates from abrasion of the stainless-steel vial and balls since the samples with small x are predominantly composed of alumina, a very abrasive milling medium.

With a starting concentration of hematite comprised between $0.12 < x \leqslant 0.50$, only alumina and broadened hematite peaks could be observed in the patterns [Figs. 1(c)–1(d)]. If any reaction between the precursors in the $(Fe_2O_3)_{0.50}(Al_2O_3)_{0.50}$ sample, for instance, effectively happened, XRD would not be able to detect it, considering the ordinary conditions in which it was applied. The broadening of hematite x-ray lines is associated with an effective particle size reduction, as well as with internal crystal strains and aluminum-substituted iron in this oxide. In fact, these situations have usually been reached through the high-energy ball-milling process.[7,8]

Room-temperature Mössbauer spectra for some selected samples are shown in Fig. 2, with the respective hyperfine magnetic field (B_{hf}) and QS distributions (histograms) as inserts in this figure. The hyperfine parameters obtained from the spectral analysis are listed in Table I. As can be observed, the spectra of samples with $x \leqslant 0.12$ [Figs. 2(a)–2(c)] were fitted with two discrete sites (a singlet and a doublet) and with B_{hf} and QS distributions, each one with a proper δ. For

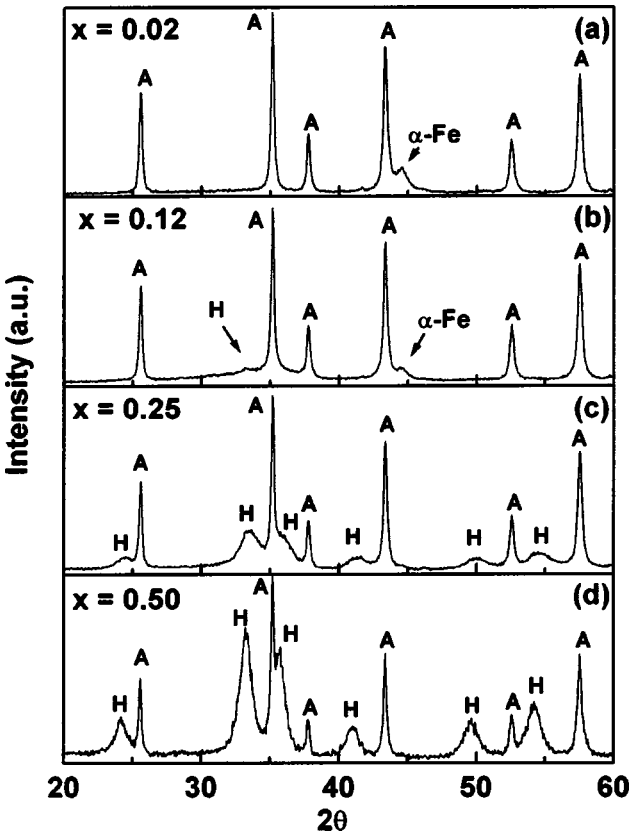

FIG. 1. X-ray diffraction patterns for $(Fe_2O_3)_x(Al_2O_3)_{1-x}$ ball-milled samples: (a) $x=0.02$, (b) $x=0.12$, (c) $x=0.25$, and (d) $x=0.50$. The A and H symbols refer to alumina (α-Al_2O_3) and hematite (α-Fe_2O_3), respectively.

$x=0.02$ and 0.10, the magnetic component has hyperfine parameters, δ and B_{hf}^{max} (i.e., the most probable field) close to those of bulk iron (α-Fe), thus corroborating with the XRD evidence for the iron presence in those samples. The broadened lines of the magnetic subspectrum may be attributed to the size distribution of iron particles and to the lattice distortions promoted by the milling process. The repeated process of breaking particles may, also, have produced a nanoscaled material with a very small grain size. This is a known product of the high-energy ball-milling process.[7–10] Thus, the single line present among the individual subspectra is attributed to SPM iron nanoprecipitates. Indeed, several authors have reported a singlet with similar values for the δ in iron implanted alumina samples[17–21] and as-sputtered $Fe:Al_2O_3$ thin films,[22] and attributed it to nanostructured iron. The same SPM phase was also detected in an earlier work during a systematic arc-melting study of $Fe_Z(Al_2O_3)_{1-Z}$, as reported by Paesano *et al.*[23] They observed that, concurrently to iron in nano and bulk forms, the spinel oxide $FeAl_2O_{3+Y}$ was formed for every iron concentration, Z, in the range $0.02 \leqslant Z \leqslant 0.60$. As performed by Paesano *et al.*, a QS distribution with a single δ was here employed to consistently fit this quadrupolar contribution. The distribution could be justified by the fact that hercynite is an inverse spinel, in which iron has several distinct neighborhoods. Furthermore, lattice defects such as strain and/or the high area/volume ratio of particles, originated by the milling process, also contribute to scatter the quadrupolar splitting. The obtained hyperfine parameters (see Table I) are, in fact, reasonably comparable to those of the hercynite spinel phase as earlier reported by other authors.[24] While δ for this mixed oxide is consistent with Fe^{2+}, the other quadrupolar component (i.e., the discrete doublet) presents hyperfine parameters that correspond to trivalent iron. Given that ball milling can break particles up to nanosized scale and dissolve mutually Fe_2O_3 and Al_2O_3, the doublet may be attributed to a paramagnetic "iron-poor" solid solution, α-$(Fe_{\Delta Y}Al_{1-\Delta Y})_2O_3$, where iron substitutes aluminum in the alumina matrix. Mixed with alumina in a relatively small starting concentration, the precursor iron oxide would be consumed in a few hours of milling. This explains why no evidence for remanent hematite in magnetically ordered bulk form could be detected by MS or XRD in samples for which $x<0.12$.

Considering the sample with $x=0.12$ [Fig. 2(c)], for which the same subspectral components of the earlier cases were used in the fitting procedure, not only one strong maximum can be observed in the magnetic field distribution but two maxima, centered around 32 and 50 T. The full magnetic contribution is, now, a combination of bulk iron (32 T) and another magnetic site (50 T), both phases strained by the mechanical process. The two distinct quadrupolar components are associated, as before, with the hercynite (QS distribution) and the earlier-mentioned solid solution (discrete doublet). It is worth noting that the total amount of iron (nano+bulk) was largely reduced, while the amount of the Fe^{3+} phase increased with x.

For $x>0.12$, the 50 T magnetic contribution will increase, while the bulk+nano iron, in the resolution-limits of the Mössbauer technique, are virtually absent. According to our proposition set out earlier, regarding the iron originating from the vial and balls, this means that α-Fe contamination now becomes low in comparison with the iron oxide content, and is very difficult to detect. Nevertheless, for $x=0.20$ [Fig. 2(d)], the hercynite Fe^{2+} quadrupolar contribution is still present, with an enlarged linewidth doublet replacing the QS distribution used for $x<0.20$. Superposed and showing an evident growth with x is the Fe^{3+} doublet belonging to the α-$(Fe_{\Delta Y}Al_{1-\Delta Y})_2O_3$ phase. The hyperfine parameters (see Table I), as well as the profile of the magnetic distribution which, for $x=0.20$, accounts for $\sim$21% of the total spectral area, reveal now more evidently than for $x=0.12$, the remains of the precursor iron oxide, probably with some aluminum substituting iron in the hematite matrix. Thus, an iron-rich solid solution, α-$(Fe_{1-\Delta W}Al_{\Delta W})_2O_3$, is supposed to occur with variable iron concentration throughout the sample and, as a result of the milling process, with a poorly crystallized structure. In our opinion, aluminum-substituted hematite is shown at around $x=0.12$ because it is not possible, as it is for smaller values of x, to completely dissolve, after 24 h of milling, such a fraction of iron oxide in aluminum oxide. Studies on several binary systems (metal +oxide/oxide+oxide) prepared in our planetary ball mill with diverse vials (e.g., hardened steel, alumina, tungsten carbide, etc.) have invariably shown that blending after a few hours of milling action on a mixing pair is maximized for solute concentrations around 10%.[25] Therefore, according to

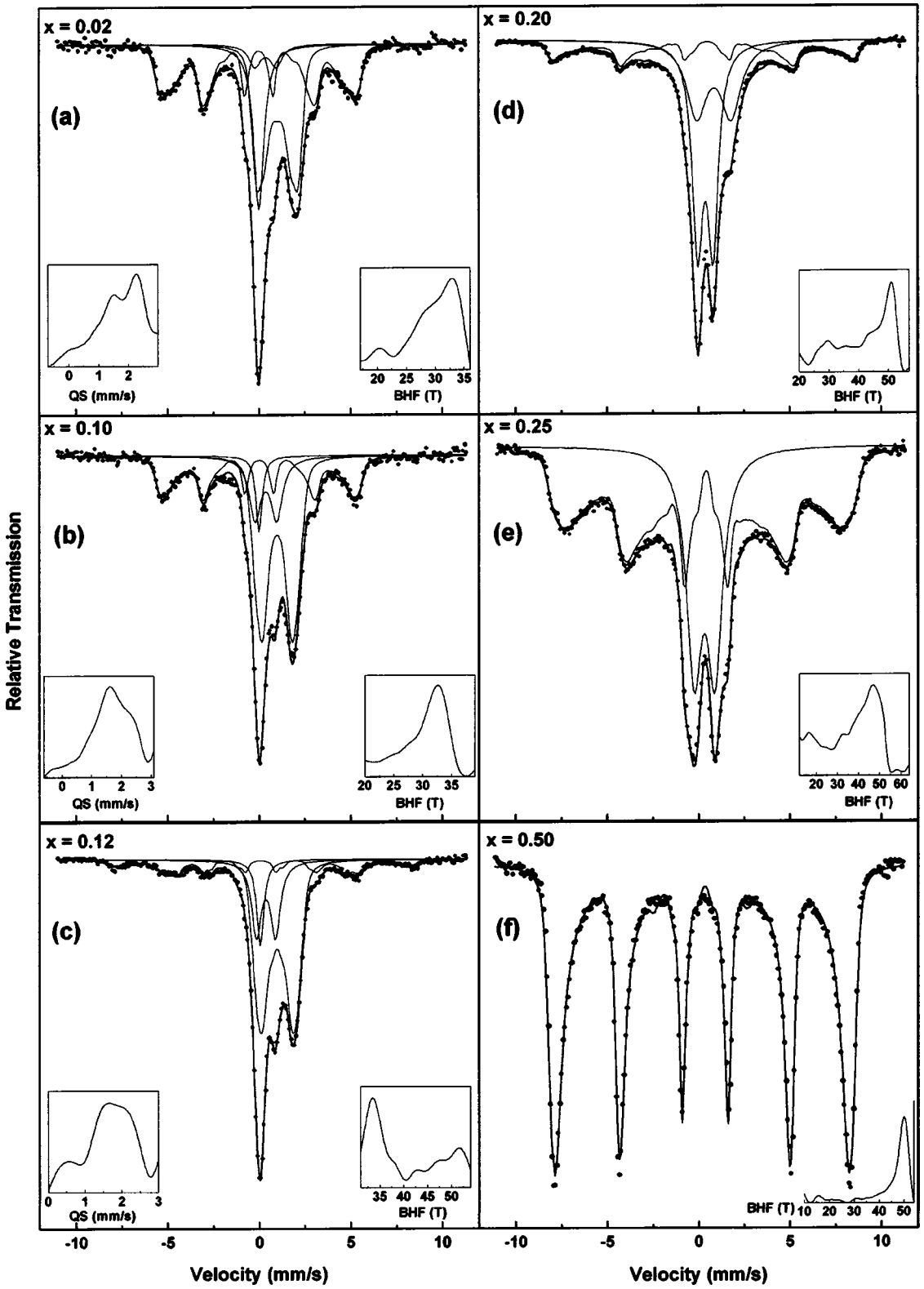

FIG. 2. Mössbauer spectra, obtained at room temperature for $(Fe_2O_3)_x(Al_2O_3)_{1-x}$ ball-milled samples: (a) $x=0.02$, (b) $x=0.10$, (c) $x=0.12$, (d) $x=0.20$, (e) $x=0.25$, and (f) $x=0.50$. Insets: quadrupole splitting and magnetic hyperfine field distributions.

our experience, above $x\sim0.10$ traces of bulk hematite should probably appear.

Strictly speaking, the α-$(Fe_{\Delta Y}Al_{1-\Delta Y})_2O_3$ and α-$(Fe_{1-\Delta W}Al_{\Delta W})_2O_3$ components are not meant to constitute two different crystallographic phases but isostructural solid solutions with different ranges of iron concentration, similarly to the phases predicted by the equilibrium phase diagram of this oxide binary system.[26] This supposition implies that the used milling apparatus with the selected settings did not provide complete mutual solubility between the

TABLE I. Mössbauer hyperfine parameters for $(Fe_2O_3)_x(Al_2O_3)_{1-x}$ ball-milled samples.

X	Subspectrum	B_{hf} (T)	IS[a] (mm/s) (± 0.02)	QS (mm/s) (± 0.02)	Area (%) (± 0.1)	Full width at half maximum (mm/s)
0.02						
	B_{hf} dist.	29.2[b]	0.00	0.00	38.4	⋯
	Fe^{3+} doublet	⋯	0.37	1.17	05.3	0.77
	Fe^{2+} QS dist.	⋯	1.01	1.68[c]	38.3	⋯
	Singlet	⋯	0.00	⋯	17.9	0.67
0.10						
	B_{hf} dist.	30.1[b]	0.00	0.00	29.5	⋯
	Fe^{3+} doublet	⋯	0.37	1.18	16.3	0.77
	Fe^{2+} QS dist.	⋯	0.98	1.64[c]	48.7	⋯
	Singlet	⋯	0.00	⋯	05.4	0.40
0.12						
	B_{hf} dist.	37.6[b]	0.03	0.05	15.5	⋯
	Fe^{3+} doublet	⋯	0.37	1.04	19.4	0.63
	Fe^{2+} QS dist.	⋯	0.98	1.62[c]	56.7	⋯
	Singlet	⋯	0.06	⋯	08.3	0.46
0.15						
	B_{hf} dist.	42.7[b]	0.32	−0.06	13.2	⋯
	Fe^{3+} doublet	⋯	0.38	0.89	51.2	0.69
	Fe^{2+} QS dist.	⋯	0.97	1.73[c]	35.6	⋯
0.20						
	B_{hf} dist.	41.5[b]	0.39	−0.20	22.5	⋯
	Fe^{3+} doublet	⋯	0.39	0.70	31.9	0.85
	Fe^{2+} doublet	⋯	0.86	1.88	45.5	1.32
0.25						
(RT)	B_{hf} dist.	36.8[b]	0.35	−0.13	67.2	⋯
	Fe^{3+} doublet	⋯	0.32	1.14	32.8	1.01
0.25						
(220 K)	B_{hf} dist.	36.4[b]	0.40	−0.15	47.6	⋯
	Sextet	50.3	0.42	−0.15	34.9	0.62
	Fe^{3+} doublet	⋯	0.37	1.29	17.5	1.00
0.25						
(6 K)	B_{hf} dist.	44.8[b]	0.46	−0.07	30.7	⋯
	Sextet	50.9	0.47	−0.11	69.3	0.52
0.30						
	B_{hf} dist.	39.0[b]	0.37	−0.14	83.8	⋯
	Fe^{3+} doublet	⋯	0.32	1.16	16.2	1.27
0.50						
	B_{hf} dist.	44.5[b]	0.37	−0.15	100.0	⋯

[a]Relative to α-Fe foil at room temperature.
[b]Average hyperfine magnetic field.
[c]Average quadrupole splitting.

oxides, although metastably extended solid solutions are expected at both extremes of the composition.[27] Due to limitations in the mutual solubility shown by the $Fe_2O_3-Al_2O_3$ system in equilibrium state, a gap between the composition ranges may be expected even for a nonequilibrium mixing process such as ball milling. In other words, we believe that a compositionally balanced iron–aluminum monophase oxide was not achieved with the applied milling conditions. Interestingly, preliminary investigations using an alumina vial in the same planetary mill have indicated that a solid solution of $(Fe_{\sim 0.50}Al_{\sim 0.50})_2O_3$ is easily accomplished after 24 h of milling.

In the intermediate concentration $x=0.25$ [Fig. 2(e)], the measured Mössbauer spectrum is very different from those previously recorded. In fact, the sextet attributed earlier to the α-$(Fe_{1-\Delta W}Al_{\Delta W})_2O_3$ solid solution phase is much more intense, though still quite broadened. This hyperfine field distribution is typical of a magnetic phase for which there was a particle size reduction until a single domain was achieved, although without completely reducing the particle size after milling times of 24 h under the blocking volume, V_C, when a magnetic phase transition (AF or WF⇒SPM) takes place.[7] As a consequence, relaxation effects may be occurring and leading to a lower (relative to the bulk hematite field, 51.5 T) average value, $\langle B_{hf} \rangle$ (see Table I). Additionally, the most probable hyperfine magnetic field B_{hf}^{max} [see the inset in Fig. 2(e)] decreased relative to the field of a graded and well

crystallized hematite because iron substitution by a nonmagnetic atom (i.e., by aluminum) causes a reduction in the magnetic hyperfine field, as previously stated by de Grave *et al.*[28–30]

One can argue about the possible formation of maghemite, as previously reported for high-energy ball-milling induced hematite phase transformations,[8,31] and whose B_{hf} is ~50 T at RT. If Mössbauer data are ambiguous on this point, the XRD data are not, since the γ-Fe_2O_3 phase pattern could not be identified in the diffractogram in Fig. 1(d).

An additional and relevant change in this spectrum [Fig. 2(e)] is the absence of the component attributed to the hercynite phase since only one doublet (Fe^{3+}) was necessary to fit it besides the magnetic distribution. The doublet, earlier assigned to the α-$(Fe_{\Delta Y}Al_{1-\Delta Y})_2O_3$ phase, showed some variation in the hyperfine parameters, smaller for δ and larger for QS, as the starting iron oxide concentration increases. This indicates that the intrinsic profile of the iron concentration may be changing with x in this solid solution, certainly getting richer in iron content.

Finally, the spectrum of the sample with composition $x=0.50$ [Fig. 2(f)] presents only a magnetic field distribution belonging to the α-$(Fe_{1-\Delta W}Al_{\Delta W})_2O_3$ phase, again with a maximum at around 50 T but with lines less broadened than those for samples with $x=0.20$ and 0.25. This shows that the iron-rich solid solution particles are larger at this starting composition, revealing how the decrease in the initial relative amount of alumina affects the grain size reduction of that solid solution. The B_{hf}^{max} of this spectrum corresponds to those reported for hematite, in which particle size reduction and some iron substitution by aluminum have weakened the hyperfine field magnitude.[7–10,28–30] The presence of the solid solution phase is corroborated by the XRD pattern [Fig. 1(d)], where intense though broadened hematite lines are observed. An attempt to impose a Fe^{3+} doublet demonstrated that such a contribution is, if any, less than 1%. This virtual absence reveals that, at this composition, the precursor iron oxide particles were scarcely dissolved in alumina.

To test our assumptions on the milling products evolution and gain some insight into the magnetic behavior of the resulting phases, the sample $(Fe_2O_3)_{0.25}(Al_2O_3)_{0.75}$ was MS characterized also in the low temperature range of 250–6 K. The 220 and 6 K spectra, together with the RT one, are shown in Fig. 3. The spectrum obtained at 220 K was fitted by adding a discrete sextet to the components used in the RT spectrum fitting. This contribution comes from the largest and/or richest iron particles of the solid solution α-$(Fe_{1-\Delta W}Al_{\Delta W})_2O_3$, which has reached saturation in terms of spontaneous magnetization. It can also be observed that the doublet area decreased in relation to the RT spectrum, indicating a progressive magnetic splitting of the α-$(Fe_{\Delta Y}Al_{1-\Delta Y})_2O_3$ component as the temperature decreases.

The 6 K experimental spectrum is a moderately broadened magnetic pattern, indicating that the RT paramagnetic (Fe^{3+}) doublet was completely led to an ordered magnetic state at this temperature. The obtained spectrum was satisfactorily fitted with a discrete sextet and a B_{hf} distribution.

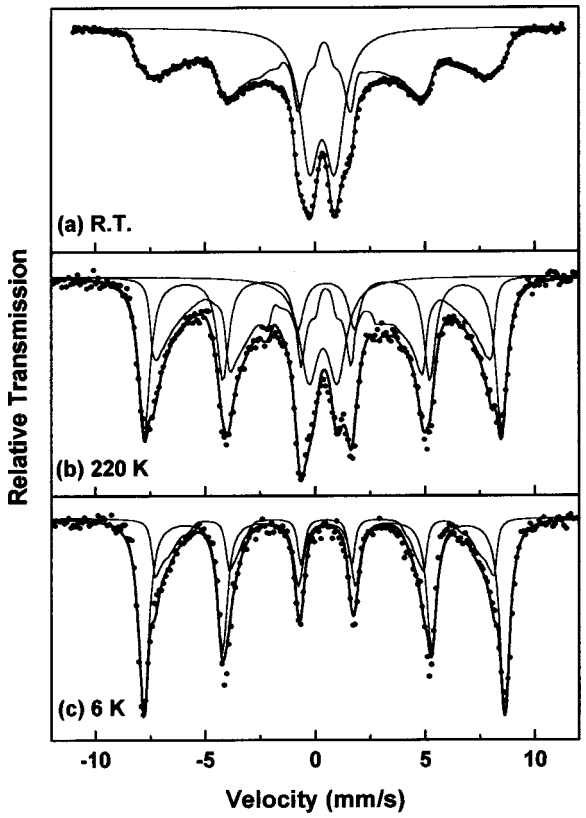

FIG. 3. Mössbauer spectra for $(Fe_2O_3)_{0.25}(Al_2O_3)_{0.75}$ ball-milled sample at room temperature (a), 220 (b), and 6 K (c).

The discrete subspectrum is, again, attributed to the α-$(Fe_{1-\Delta W}Al_{\Delta W})_2O_3$ phase, which now shows a more defined pattern (i.e., smaller linewidth) and a still larger hyperfine field. This is a consequence of the decreasing relaxation time that, at 6 K, is definitely shorter than the time scale for Mössbauer measurements. In other words, the blocking temperature for Mössbauer experiments is above 6 K for the milled phase α-$(Fe_{1-\Delta W}Al_{\Delta W})_2O_3$. Its hyperfine parameters are very close to those reported by Randrianantoandro *et al.*[8] for ball-milled hematite. It is significant that the area ratio at 6 K shown by the two different magnetic components is nearly the same as that presented at RT (see Table I), between the magnetic and nonmagnetic components. This verifies the existence of the compositional bimodal distribution previously pointed out and represented by the α-$(Fe_{\Delta Y}Al_{1-\Delta Y})_2O_3$ (weakest field component/B_{hf} distribution at 6 K) and α-$(Fe_{1-\Delta W}Al_{\Delta W})_2O_3$ (strongest field component/discrete field at 6 K) phases.

Another question related to the nature of the magnetic ordering of the α-$(Fe_{1-\Delta W}Al_{\Delta W})O_3$ solid solution is whether it aligns AF or WF. Bulk α-Fe_2O_3 undergoes a Morin transition at nearly 260 K as well established in the literature.[11] However, by reducing the particle size or introducing substitutional aluminum in bulk hematite, T_M decreases or is even suppressed.[30] Mössbauer data, particularly the QS sign, were correlated with the magnetic order in a system of the α-$(Fe,Al)_2O_3$ type by de Grave *et al.*,[30] with a negative QS implying a WF order. Consistent with this interpretation, our Mössbauer data indicate a WF order for the

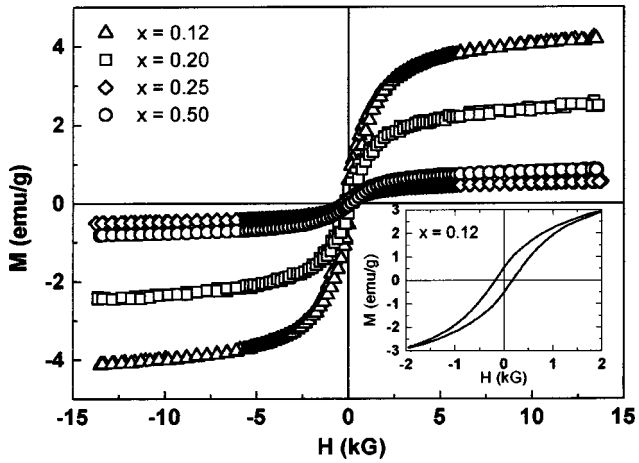

FIG. 4. Magnetic hysteresis curves, measured at room temperature, for $(Fe_2O_3)_x(Al_2O_3)_{1-x}$ ball-milled samples: $x=0.12$, $x=0.20$, $x=0.25$, and $x=0.50$. Inset: Loop $(Fe_2O_3)_{0.12}(Al_2O_3)_{0.88}$ sample at low magnetic field levels.

iron-rich solid solution, since QS is always negative from $x=0.15$ up to $x=0.50$, at RT and low temperatures.

The magnetization versus magnetic field curves, $M(H)$, for samples with $x \geqslant 0.12$, are shown in Fig. 4. As can be seen, particularly for $x=0.12$ (inset), besides a general SPM character, some hysteretic behavior is revealed in all compositions. For every x, it can be observed that the magnetization curves start to increase rapidly with magnetic field at low field levels. With field amplitude increasing over ~ 2 kG, a curvature starts to appear in all magnetization curves, being followed by an almost linear growth behavior, without saturation at higher field levels. The hysteretic contribution may be partially attributed to α-$(Fe_{1-\Delta W}Al_{\Delta W})_2O_3$ previously identified in the MS characterization as a magnetically ordered phase at RT. On the other hand, the SPM component may be attributed to the very fine particles of the α-$(Fe_{1-\Delta W}Al_{\Delta W})_2O_3$ phase, for which the relaxation time is shorter than the time for magnetization measurements (~ 100 s).[23] Being paramagnetic at RT, the α-$(Fe_{\Delta Y}Al_{1-\Delta Y})_2O_3$ phase may be making a small contribution to the magnetization curve, $M_P(H)$, which varies linearly with H. We also observe that $M(H)$ decreases rapidly with the concentration and increases for $x>0.25$, for any fixed H. The initial lowering is a consequence of progressive reduction in the fraction of the α-Fe incorporated in the sample by abrasion of the vial and balls. The further increase is credited to the growth of the relative amount of α-$(Fe_{1-\Delta W}Al_{\Delta W})_2O_3$ as revealed by MS.

IV. CONCLUSIONS

The products obtained through 24 h of high-energy ball milling of the $(\alpha\text{-}Fe_2O_3)_x(\alpha\text{-}Al_2O_3)_{100-x}$ system are dependent on the hematite starting concentration, x. However, alumina surplus is always observed as well as particle size reduction for every present phase. For samples with low solute concentrations (i.e., $x \leqslant 0.12$), contamination by α-Fe deriving from the stainless-steel vial and balls was detected. The spinel $FeAl_2O_4$ phase, whose presence can be associated with available metallic iron, was also identified, at least up to $x=0.20$. A bimodal distribution, concerning the aluminum (iron) concentration in hematite (corundum) lattice, was produced by ball milling giving rise to the solid solutions α-$(Fe_{1-\Delta W}Al_{\Delta W})O_3$ and α-$(Fe_{\Delta Y}Al_{1-\Delta Y})_2O_3$. The relative amounts of both components vary with the sample nominal starting concentration, the iron-richest component growing whereas the iron-poorest diminishing with increasing x. At room temperature, the former is weak ferromagnetic, presenting a hyperfine field distribution, and the latter is paramagnetic, but both solid solutions are magnetically well ordered at 6 K. The Morin temperature is not observed down to 6 K or was suppressed in the α-$(Fe_{1-\Delta W}Al_{\Delta W})O_3$ solid solution due to an effective grain size reduction in addition to the substitution of a magnetic atom (Fe) by a nonmagnetic atom (Al) in the precursor iron oxide.

ACKNOWLEDGMENTS

The authors would like to thank the CAPES (PROCAD, Contract No. 0021/00-8) and CNPq Brazilian agencies for financial support.

[1] C. Suryanarayana, Prog. Mater. Sci. **46**, 1 (2001), and references therein.
[2] W. A. Kaczmarek, J. Mater. Sci. **34**, 5271 (1996).
[3] K. Santha, G. N. Subbanna, and K. B. R. Varma, J. Solid State Chem. **142**, 41 (1999).
[4] A. Calka and D. Wexler, Nature (London) **419**, 147 (2002).
[5] M. Zdujic, C. Jovalekic, Lj. Karanovic, M. Mitric, D. Poleti, and D. Skala, Mater. Sci. Eng., A **245**, 109 (1998).
[6] M. Zdujic, C. Jovalekic, and M. Mitric, Mater. Sci. Eng., A **262**, 204 (1999).
[7] R. A. Borzi, S. J. Stewart, G. Punte, R. C. Mercader, M. Vasquez-Mansilla, R. D. Zysler, and E. D. Cabanillas, J. Magn. Magn. Mater. **205**, 234 (1999).
[8] N. Randrianantoandro, A. M. Mercier, M. Hervieu, and J. M. Greneche, Mater. Lett. **47**, 150 (2001).
[9] S. Bid, A. Banerjee, S. Kumar, S. K. Pradhan, U. De, and D. Banerjee, J. Alloys Compd. **326**, 292 (2001).
[10] E. Petrovsky, M. D. Alcala, J. M. Criado, T. Grygar, A. Kapicka, and J. Subrt, J. Magn. Magn. Mater. **210**, 257 (2000).
[11] F. J. Morin, Phys. Rev. **78**, 819 (1950).
[12] J. L. Dormann, D. Fiorani, and E. Tronc, Adv. Chem. Phys. **98**, 283 (1997).
[13] J. Ding, P. G. McCormick, and R. Street, J. Magn. Magn. Mater. **171**, 309 (1997).
[14] S. Bhagwat, S. Joshi, S. B. Ogale, G. Marest, A. Benyagoub, N. Mancoffre, and F. Thimon, J. Appl. Phys. **79**, 4141 (1996).
[15] L. Takacs, Mater. Lett. **13**, 119 (1992).
[16] L. H. Bowen and E. De Grave, J. Magn. Magn. Mater. **139**, 6 (1995).
[17] C. J. McHargue, G. C. Farlow, P. S. Sklad, C. W. White, A. Perez, N. Kornilios, and G. Marest, Nucl. Instrum. Methods Phys. Res. B **19/20**, 813 (1987).
[18] C. Donnet, H. Jaffrezic, G. Marest, N. Moncoffre, and J. Tousset, Nucl. Instrum. Methods Phys. Res. B **50**, 410 (1990).
[19] C. Donnet, G. Marest, N. Moncoffre, and J. Tousset, Nucl. Instrum. Methods Phys. Res. B **59/60**, 1177 (1991).
[20] C. J. McHargue, P. S. Sklad, C. W. White, G. C. Farlow, A. Perez, and G. Marest, J. Mater. Res. **6**, 2145 (1991).
[21] C. J. McHargue, P. S. Sklad, C. W. White, J. C. McCallum, A. Perez, and G. Marest, J. Mater. Res. **6**, 2160 (1991).
[22] F. Thimon, G. Marest, and N. Moncroffre, Nucl. Instrum. Methods Phys. Res. B **80/81**, 1241 (1993).
[23] A. Paesano, Jr., C. K. Matsuda, J. B. M. da Cunha, M. A. Z. Vasconcellos, B. Hallouche, and S. L. Silva, J. Magn. Magn. Mater. **264**, 264 (2003).
[24] L. Larsson, H. ST. O'Neil, and H. Annersten, Eur. J. Mineral. **6**, 39 (1994), and references therein.

[25] Unpublished data.
[26] A. Muan, Am. J. Sci. **256**, 420 (1958).
[27] J. Z. Jiang, S. Morup, and S. Linderoth, Mater. Sci. Forum **225**, 489 (1996).
[28] E. De Grave, L. H. Bowen, D. D. Amarasiriwardena, and R. E. Vanderberghe, J. Magn. Magn. Mater. **72**, 129 (1988).
[29] E. De Grave, L. H. Bowen, R. Vochten, and R. E. Vanderberghe, J. Magn. Magn. Mater. **72**, 141 (1988).
[30] E. De Grave, L. H. Bowen, and S. B. Weed, J. Magn. Magn. Mater. **27**, 98 (1982).
[31] N. N. Greenwood and T. C. Gibb, *Mössbauer Spectroscopy* (Chapman and Hall, London, 1971).